

Unraveling the hardness of a borophene-based compound

N. Gonzalez Szwacki

Institute of Theoretical Physics, Faculty of Physics, University of Warsaw, ul. Pasteura 5, PL-02-093 Warsaw, Poland

gonz@fuw.edu.pl

ABSTRACT

Two-dimensional systems have strengthened their position as one of the key materials for novel applications. Very recently, boron joined the distinguished group of elements that are confirmed to possess 2D allotropes, named borophenes. In this work, we explore the stability and hardness of the highest boride of tungsten, which is regarded as built of borophenes separated by metal atoms. We show that WB_{3+x} has Vickers hardnesses approaching 40 GPa only for small values of x . The insertion of extra boron atoms is, in general, detrimental for WB_3 in terms of hardness since leads to the formation of quasi-planar boron sheets that are less tightly connected with the adjacent W layers. Very high concentrations of boron ($x \approx 1$), give rise to a soft (Vickers hardness of about 8 GPa) and unstable $hP20-WB_4$ structure that can be considered as built of quasi-planar boron α -sheets separated by graphitic W layers. On the other hand, we show that the formation of tungsten vacancies brings on structures, e.g. $W_{0.75}B_{3+x}$, with Vickers hardnesses that are less sensitive to variations in the boron content and are close in value to the experimentally reported load-independent values above 20 GPa.

Introduction

The highest boride of tungsten – often referred to as tungsten tetraboride – is recently best explored for its potential applications as superhard material, however made its first appearance in the literature in 1961, when Chretien and Helgorsky¹ did the first attempt to find its structure. Years later Romans and Krug² reported that WB_4 has a hexagonal structure of 20 atoms per unit cell and lattice constants of 5.2 and 6.34 Å for a and c , respectively. The space group of this structure was determined to be $P6_3/mmc$. The $hP20-WB_4$ structure serves now as a reference structure for almost all subsequent experimental studies related to boron-rich materials with a WB_4 -like structure.^{3–7} The mechanical properties of WB_4 were first determined by Gu *et al.*³ who reported Vickers hardness (H_V) values of 46.2 and 31.8 GPa under applied loads of 0.49 and 4.90 N, respectively, measured by the microindentation technic. Subsequently, Mohammadi *et al.*⁵ also measured the hardness by microindentation method and reported H_V values of 43.3 and 28.1 GPa at low (0.49 N) and high (4.90 N) loads, respectively. More recently, the Vickers hardness for $W_{0.85}B_3$ was reported by Tao *et al.*⁸ to be 42.0 and 25.5 GPa under applied loads of 0.098 and 4.90 N, respectively. Finally, Lech *et al.*⁹ determined the maximum nanoindentation hardness of $W_{0.82}B_{3.54}$ (at a penetration depth of 95.25 nm) to be 41.7 GPa. It is generally accepted that a reliable hardness of a material can be determined from the asymptotic hardness region achieved at high loads.¹⁰ The quite large differences between the H_V values reported for WB_4 , especially for high loads, can be attributed to differences in the amount of boron contamination and/or presence of tungsten vacancies, which were experimentally seen in the studied samples.⁹ By exploring structures with different compositions, we are able to explain on the theoretical ground the apparent differences between the reported experimental results.

The common description of $hP20-WB_4$ that can be found in the literature is that this structure consists of graphitic boron layers separated by graphitic layers of W atoms like in the $hP16-WB_3$ structure but with additional B_2 dimers located between boron sheets and aligned along the c -axis (see Fig. 1a). This description, although very elegant, is completely decoupled from more recent investigations related to 2D boron crystals.^{11,12} An ‘updated’ view to $hP20-WB_4$ would be that it is a structure consisting of a sequence of quasi-planar boron α -sheets separated by graphitic W layers. Extensive theoretical investigations have proved, however, that the stoichiometric $hP20-WB_4$ structure is thermodynamically and dynamically unstable. Its calculated enthalpy of formation is positive, with a value of 0.4 eV/atom,¹³ and from its phonon dispersion the structure was shown to be highly unstable.¹⁴ In fact, we argue that the formation of stable quasi-planar boron layers within the $hP20-WB_4$ structure is the main reason for the instability of this and related boron rich structures. Therefore $hP20-WB_4$ is in that view a nonexistent structure.

In more recent reports,^{13,15} the highest borides of tungsten are described as $hP16-WB_3$ structures contaminated with additional boron atoms. The exact position of the boron atoms in the crystal lattice are difficult to be determined experimentally

because of the large mass difference between W and B atoms.¹⁵ Therefore, the combination of theory and experiment is essential for the understanding of the observed findings. Since in the experiment the $hP16\text{-WB}_3$ structure is not only contaminated with boron atoms but also, to some extent, possesses tungsten vacancies,^{8,9,16} in this work a more precise notation is used when referring to the highest boride of tungsten, namely $W_{1-y}B_{3+x}$, to underline the existence of W vacancies and explore their influence on the stability and properties of WB_{3+x} .

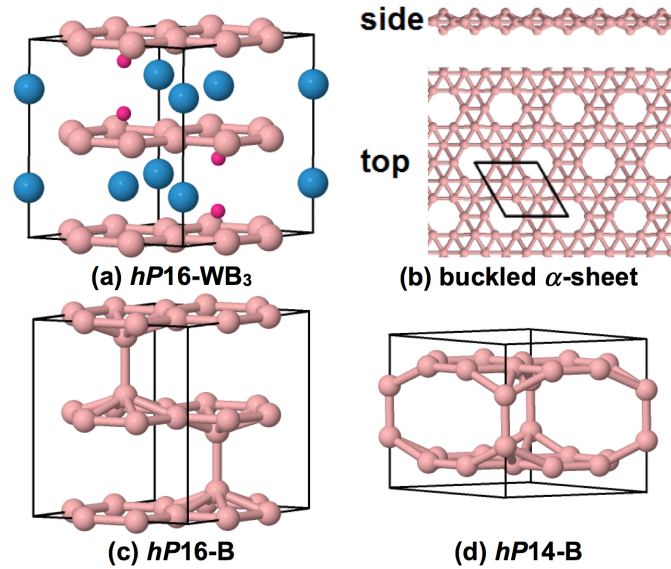


Figure 1. (Color online). (a) The $hP16\text{-WB}_3$ structure. The large and small spheres represent W and B atoms, respectively. The small red dots indicate the position of the 4 extra boron atoms that are present in the $hP20\text{-WB}_4$ structure. (b) Buckled boron α -sheet present in the $hP20\text{-WB}_4$ structure. (c) The $hP16\text{-B}$ structure that is obtained by removing all the tungsten atoms from $hP20\text{-WB}_3$. (d) The $hP14\text{-B}$ structure that derives from $hP16\text{-B}$ by removing one of the two dimers.

Table 1. Phases, occupations relative to the $P6_3/mmc$ space group, lattice constants, and resulting space groups of the most stable structures at a given composition.

Phase	Occ. relative to $P6_3/mmc$				a (Å)	c (Å)	Resulting space group
	W1 (2c)	W2 (2b)	B1 (12i)	B2 (4f)			
WB_3	1	1	1	0	5.171	6.228	$P6_3/mmc$
$WB_{3.25}$	1	1	1	0.25	5.173	6.405	$P3m1$
$WB_{3.5}$	1	1	1	0.5	5.195	6.398	$P3m1$
WB_4	1	1	1	1	5.327	6.334	$P6_3/mmc$
$W_{0.75}B_3$	1	0.5	1	0	5.416	5.271	$P6/mmm$
$W_{0.75}B_{3.25}$	0.5	1	1	0.25	5.144	6.305	$P3m1$
$W_{0.75}B_{3.5}$	1	0.5	1	0.5	5.139	6.398	$P\bar{6}m2$
$W_{0.75}B_{3.75}$	1	0.5	1	0.75	5.211	6.291	$P3m1$

Results

The structure of $W_{1-y}B_{3+x}$. The highest boride of tungsten are obtained starting from $hP16\text{-WB}_3$ by adding additional boron atoms at the positions shown in red in Fig. 1a and/or by selective removal of W atoms. The fully ‘packed’ structure is the $hP20\text{-WB}_4$ structure that has buckled boron α -sheets separated by W layers. The buckling height is 1.49 Å and is larger than that of the freestanding triangular boron sheet (0.82 Å¹⁷). The complete removal of all the W atoms from $hP20\text{-WB}_4$ leads to the all-boron structure that consists of 16 atoms per unit cell and is shown in Fig. 1c. This structure is nothing more than a sequence of quasi-planar boron α -sheets arranged in such a way that the boron atoms that stick out of the graphitic frame face each other forming dimers. In the same way, we can describe the $hP20\text{-WB}_4$ structure but this time the boron α -sheets are

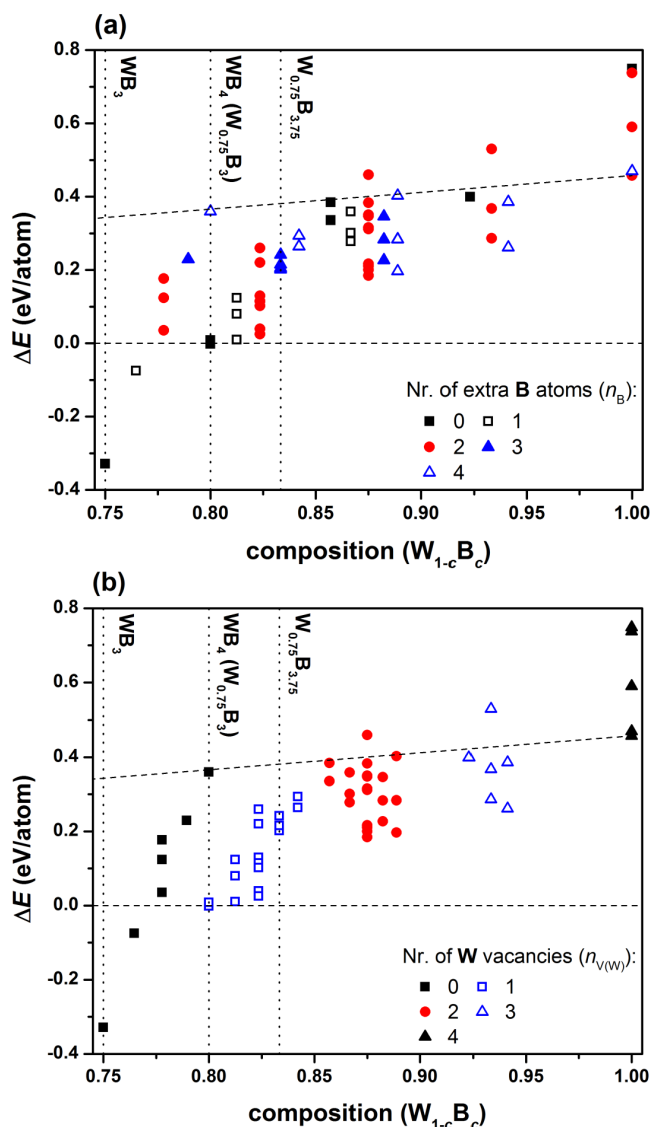


Figure 2. (Color online). Enthalpies of formation for structures derived from $hP16-WB_3$ by selective removal of W atoms and/or contamination by additional B atoms. The vertical dotted lines correspond to compositions that were reported in the literature.

separated by W graphitic layers. The $hP16-B$ structure is less stable than the α -rhombohedral boron ($hR12-B$) by 0.47 eV/atom. Interestingly enough, by removing one of the boron dimers in $hP16-B$ a slightly more stable (by 12 meV/atom) structure shown in Fig. 1c is obtained. The $hP16-B$ and $hP14-B$ structures have $P6_3/mmc$ and $P6/mmm$ space groups, respectively, and $a = 5.034 \text{ \AA}$, $c = 6.166 \text{ \AA}$ and $a = 5.081 \text{ \AA}$, $c = 5.195 \text{ \AA}$ lattice constants, respectively.

Stability of the compounds. To explore the relative stability of the generated structures, we calculate for each structure its enthalpy of formation per atom, ΔE . The ΔE values are calculated relative to the chemical potentials of W and B atoms obtained based on the body-centered cubic tungsten ($cI2-W$) and α -rhombohedral boron ($hR12-B$), respectively. The results of ΔE for $W_{1-c}B_c$ versus composition c are summarized in Figs. 2a and 2b. All the structures that have enthalpies of formation above the horizontal dashed lines in Figs. 2a and 2b are, in principle, thermodynamically unstable. It is instructive, however, to draw also a line that connects $cI2-W$ with $hP14-B$, what is shown in Figs. 2a and 2b by a dashed line that is above the horizontal dashed line. The enthalpies of formation of almost all the considered structures $W_{1-y}B_{3+x}$ are located below the $cI2-W \leftrightarrow hP14-B$ line. This means that the incorporation of W atoms in between boron sheets is energetically favourable. The enthalpies of formation versus composition are presented in two ways. In Fig. 2a, we organized the results according to the number of extra boron atoms, n_B , in $W_{1-y}B_{3+x}$ relative to $hP16-WB_3$. In Fig. 2b, the same results have been organized emphasizing the number of W vacancies in $W_{1-y}B_{3+x}$ also relative to $hP16-WB_3$. It is clear from Fig. 2a that negative enthalpies of formation

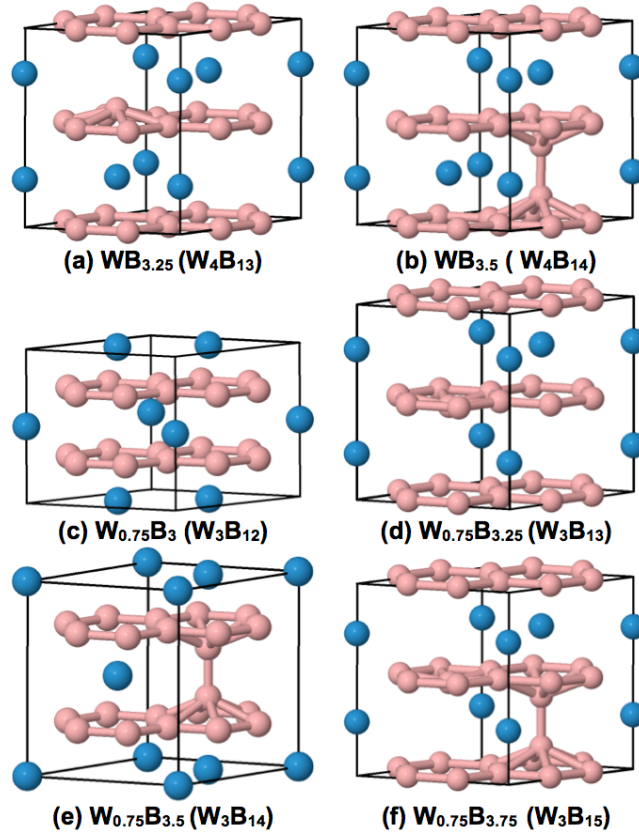


Figure 3. (Color online). The crystal structure of several boron rich phases of the W-B system. The large and small spheres represent W and B atoms, respectively. The W_mB_n notation in parenthesis shows the number of W and B atoms in the unit cell.

or positive ΔE but close to 0, have structures with none or no more than 2 extra B atoms. The cases with 3 and 4 extra B atoms have $\Delta E \simeq 0.2$ eV/atom or larger. This also includes the highly debated *hP20*-WB₄ structure ($\Delta E = 0.36$ eV/atom). From Fig. 2b, we can learn that the only relevant cases are those for which the number of W vacancies, $n_{V(W)}$, is 0 or 1, since among those cases we can find structures with negative or close to 0 enthalpies of formation. Combining all the information coming from Fig. 2, we choose 8 structures that in principle can be important to understand experimental results. Six of those structures are shown in Fig. 3. For each relevant composition c , we choose the structure with the lowest enthalpy of formation. The relevant structures (the highest boride of tungsten) are those with c ranging from 0.75 (WB₃) to 0.83 (W_{0.75}B_{3.75}). The highest c is chosen following Ref.⁹.

The lattice constants and symmetry of the structures shown in Fig. 3 are summarized in Tab. I. In this table, we also include, for each structure, the occupations of the B and W atoms relative to the $P6_3/mmc$ space group. It is important to notice that if we exclude the case of W_{0.75}B₃ (that appears not to match the others) and take the average of all the rest lattice constants listed in Tab. I, we get 5.194 and 6.337 Å for a and c , respectively, that is, values that match very well those reported in the experiment (5.2 and 6.34 Å for a and c , respectively⁹). This may suggest that in the experiment is observed a non-stoichiometric structure with a random distribution of both the extra boron atoms and W vacancies and may further explain the difficulties in the interpretations of X-ray and neutron diffraction data.⁹

Mechanical properties of the compounds. The elastic properties of the studied structures are summarized in Tab. II, whereas the plot of the Vickers hardness versus composition is shown in Fig. 4. From this figure, we see that only stoichiometric WB₃ (*hP16*-WB₃) can be considered as superhard material. The hardness is however affected by contamination by extra B atoms. This is clearly seen in Fig. 4 for WB_{3+x}, for which the Vickers hardness changes from ~ 40 to ~ 8 GPa for an increase of the B content by 5%. For the tungsten-deficient structures W_{0.75}B_{3+x} the picture is different, namely, we obtain smaller variations of the Vickers hardness with the increase of B content (see Fig. 4). Most of the considered structures have Vickers hardnesses larger or equal to 20 GPa, what means that the highest boride of tungsten is a hard material but not superhard (at least in the range of considered compositions). A particularly soft structure is *hP20*-WB₄, which has a comparable bulk modulus to that of *hP16*-WB₃ but much smaller shear modulus (see Tab. II). The softening of WB₄ may be attributed to the formation of stable 2D boron layers (α -sheets) which are less tightly bound to the tungsten layers. The average nearest neighbour W–B

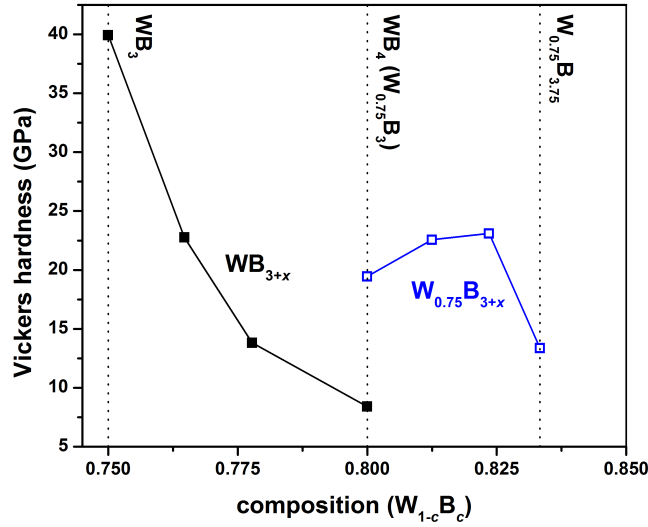


Figure 4. (Color online). Vickers hardnesses calculated for the most stable structures at a given composition. The filled and open squares correspond to structures of the WB_{3+x} and $W_{0.75}B_{3+x}$ type, respectively.

Table 2. Number of W vacancies $n_{V(W)}$, number of extra B atoms n_B , bulk modulus B (GPa), shear modulus G (GPa), Young's modulus E (GPa), Poisson's ratio ν , and Vickers hardness H_V (GPa) for several $W_{1-y}B_{3+x}$ structures.

Phase	$n_{V(W)}$	n_B	B	G	E	ν	H_V
WB ₃	0	0	315	266	622	0.17	39.9
WB _{3.25}	0	1	283	185	456	0.23	22.8
WB _{3.5}	0	2	317	156	403	0.29	13.8
WB ₄	0	4	321	126	335	0.33	8.4
W _{0.75} B ₃	1	0	289	173	433	0.25	19.5
W _{0.75} B _{3.25}	1	1	254	171	419	0.22	22.6
W _{0.75} B _{3.5}	1	2	279	184	453	0.23	23.1
W _{0.75} B _{3.75}	1	3	249	131	334	0.28	13.4

distance is 2.324 and 2.383 Å in WB₃ and WB₄, respectively, what reflects the weakening of the W–B bond in WB₄ with respect to WB₃.

In summary, we show that the insertion of extra boron atoms into the WB₃ structure is, in general, energetically unfavourable and lowers its shear modulus while keeping a high value for the bulk modulus, what effectively brings to a softer material. A high degree of boron contamination leads to the formation of quasi-planar boron α -sheets separated by graphitic W layers in WB₄. More stable and harder than WB₄ are structures of the $W_{1-y}B_{3+x}$ type, in which boron contamination is accompanied by a presence of tungsten vacancies. Finally, the formation of tungsten vacancies gives rise to structures (e.g. $W_{0.75}B_{3+x}$) with Vickers hardnesses that are less sensitive to variations in the boron content and are close in value to the experimentally reported load-independent values above 20 GPa. Our results should provide guidance for the experiment in the design of new ways of WB₄ synthesis.

Methods

Our first principles calculations are based on density functional theory (DFT) and the projector augmented wave (PAW) method as implemented in the Quantum ESPRESSO simulation package.¹⁸ For the exchange and correlation functional, we use a revised Perdew-Burke-Ernzerhof spin-polarized generalized gradient approximation (PBEsol-GGA) functional. The plane-wave basis set is converged using a 40 Ry energy cutoff. A $8 \times 8 \times 8$ k -point mesh and a Gaussian smearing of 0.005 Ry is used in the Brillouin Zone integration. The calculations are done using supercells containing up to 20 atoms. For each considered structure, we do a full atomic position and lattice parameter relaxation.

A total of 60 low-energy $W_{1-c}B_c$ structures with high boron content c are selected by using the cluster-expansion method implemented in the Alloy-Theoretic Automated Toolkit (ATAT).¹⁹ The elastic properties of the most stable structures are calculated using the ElaStic code.²⁰ To compute the Vickers hardness, we employ the semi-empirical hardness model proposed

by Chen *et al.*²¹ that correlates hardness with the elastic properties of the material. According to this model the expression for hardness is $H_V = 2(k^2G)^{0.585} - 3$, where G and k are the shear modulus and Pugh modulus ratio ($k = G/B$, $B =$ bulk modulus), respectively.

References

1. Chretien, A. & Helgorsky, J. Borides of molybdenum and tungsten, MoB₄ and WB₄; new compounds. *Compt. Rend.* **252**, 742–744 (1961).
2. Romans, P. A. & Krug, M. P. Composition and crystallographic data for the highest boride of tungsten. *Acta Crystallogr.* **20**, 313–315 (1966). URL <http://dx.doi.org/10.1107/S0365110X6600063X>. DOI 10.1107/S0365110X6600063X.
3. Gu, Q., Krauss, G. & Steurer, W. Transition metal borides: Superhard versus ultra-incompressible. *Adv. Mater.* **20**, 3620–3626 (2008). URL <http://dx.doi.org/10.1002/adma.200703025>. DOI 10.1002/adma.200703025.
4. Liu, C. *et al.* Low-compressibility of tungsten tetraboride: a high pressure X-ray diffraction study. *High Pres. Res.* **31**, 275–282 (2011). URL <http://dx.doi.org/10.1080/08957959.2011.582871>. DOI 10.1080/08957959.2011.582871.
5. Mohammadi, R. *et al.* Tungsten tetraboride, an inexpensive superhard material. *Proc. Natl. Acad. Sci. USA* **108**, 10958–10962 (2011). URL <http://www.pnas.org/content/108/27/10958.abstract>. DOI 10.1073/pnas.1102636108.
6. Xie, M. *et al.* Exploring the high-pressure behavior of superhard tungsten tetraboride. *Phys. Rev. B* **85**, 064118 (2012). URL <http://link.aps.org/doi/10.1103/PhysRevB.85.064118>. DOI 10.1103/PhysRevB.85.064118.
7. Xiong, L. *et al.* Radial x-ray diffraction of tungsten tetraboride to 86 GPa under nonhydrostatic compression. *J. Appl. Phys.* **113**, 033507 (2013). URL <http://scitation.aip.org/content/aip/journal/jap/113/3/10.1063/1.4775482>. DOI <http://dx.doi.org/10.1063/1.4775482>.
8. Tao, Q. *et al.* Exploring hardness and the distorted sp^2 hybridization of B–B bonds in WB₃. *Chem. Mater.* **26**, 5297–5302 (2014). URL <http://dx.doi.org/10.1021/cm5021806>. DOI 10.1021/cm5021806.
9. Lech, A. T., Turner, C. L., Mohammadi, R., Tolbert, S. H. & Kaner, R. B. Structure of superhard tungsten tetraboride: A missing link between MB₂ and MB₁₂ higher borides. *Proc. Natl. Acad. Sci. USA* **112**, 3223–3228 (2015). URL <http://www.pnas.org/content/112/11/3223.abstract>. DOI 10.1073/pnas.1415018112.
10. Tian, Y., Xu, B. & Zhao, Z. Microscopic theory of hardness and design of novel superhard crystals. *Int. J. Refract. Metal Hard Mater.* **33**, 93–106 (2012). URL <http://www.sciencedirect.com/science/article/pii/S026343681200042X>. DOI <http://dx.doi.org/10.1016/j.ijrmhm.2012.02.021>.
11. Tang, H. & Ismail-Beigi, S. Novel precursors for boron nanotubes: The competition of two-center and three-center bonding in boron sheets. *Phys. Rev. Lett.* **99**, 115501 (2007). URL <http://link.aps.org/doi/10.1103/PhysRevLett.99.115501>. DOI 10.1103/PhysRevLett.99.115501.
12. Feng, B. *et al.* Experimental realization of two-dimensional boron sheets. *Nat. Chem.* **8**, 563–568 (2016). URL <http://dx.doi.org/10.1038/nchem.2491>. Article.
13. Cheng, X.-Y., Chen, X.-Q., Li, D.-Z. & Li, Y.-Y. Computational materials discovery: the case of the W–B system. *Acta Crystallogr. C* **70**, 85–103 (2014). URL <https://doi.org/10.1107/S2053229613027551>. DOI 10.1107/S2053229613027551.
14. Zhang, R. F. *et al.* Stability and strength of transition-metal tetraborides and triborides. *Phys. Rev. Lett.* **108**, 255502 (2012). URL <http://link.aps.org/doi/10.1103/PhysRevLett.108.255502>. DOI 10.1103/PhysRevLett.108.255502.
15. Cheng, X. *et al.* Interstitial-boron solution strengthened WB_{3+x}. *Appl. Phys. Lett.* **103**, 171903 (2013). URL <http://scitation.aip.org/content/aip/journal/apl/103/17/10.1063/1.4826485>. DOI <http://dx.doi.org/10.1063/1.4826485>.
16. Zeiringer, I. *et al.* Crystal structure of W_{1-x}B₃ and phase equilibria in the boron-rich part of the systems Mo–Rh–B and W–{Ru,Os,Rh,Ir,Ni,Pd,Pt}–B. *J. Phase Equilibria Diffus.* **35**, 384–395 (2014). URL <http://dx.doi.org/10.1007/s11669-014-0291-0>. DOI 10.1007/s11669-014-0291-0.

17. Kunstmann, J. & Quandt, A. Broad boron sheets and boron nanotubes: An *ab initio* study of structural, electronic, and mechanical properties. *Phys. Rev. B* **74**, 035413 (2006). URL <http://link.aps.org/doi/10.1103/PhysRevB.74.035413>. DOI 10.1103/PhysRevB.74.035413.
18. Giannozzi, P. *et al.* QUANTUM ESPRESSO: a modular and open-source software project for quantum simulations of materials. *J. Phys. Condens. Matter* **21**, 395502 (2009). URL <http://stacks.iop.org/0953-8984/21/i=39/a=395502>. DOI <http://dx.doi.org/10.1088/0953-8984/21/39/395502>.
19. van de Walle, A., Asta, M. & Ceder, G. The alloy theoretic automated toolkit: A user guide. *Calphad* **26**, 539 – 553 (2002). URL <http://www.sciencedirect.com/science/article/pii/S0364591602800062>. DOI [http://dx.doi.org/10.1016/S0364-5916\(02\)80006-2](http://dx.doi.org/10.1016/S0364-5916(02)80006-2).
20. Golezorkhtabar, R., Pavone, P., Spitaler, J., Puschnig, P. & Draxl, C. ElaStic: A tool for calculating second-order elastic constants from first principles. *Comput. Phys. Commun.* **184**, 1861–1873 (2013). URL <http://www.sciencedirect.com/science/article/pii/S0010465513001070>. DOI <http://dx.doi.org/10.1016/j.cpc.2013.03.010>.
21. Chen, X.-Q., Niu, H., Li, D. & Li, Y. Modeling hardness of polycrystalline materials and bulk metallic glasses. *Intermetallics* **19**, 1275–1281 (2011). URL <http://www.sciencedirect.com/science/article/pii/S0966979511000987>. DOI <http://dx.doi.org/10.1016/j.intermet.2011.03.026>.

Acknowledgements

The author gratefully acknowledge the support of the National Research Council (NCN) through the grant UMO-2013/11/B/ST3/04273 and the access to the computing facilities of the Interdisciplinary Center of Modeling at the University of Warsaw.

Author Contribution statement

NGSz did the calculations and analysis, wrote and reviewed the manuscript, and prepared all the figures.

Competing financial interests

The author declare no competing financial interests.